Inorg. Chem. **2008**, *47*, 5841−5849

Direct Comparison of the Magnetic and Electronic Properties of Samarocene and Ytterbocene Terpyridine Complexes

Jacqueline M. Veauthier, Eric J. Schelter, Christin N. Carlson, Brian L. Scott, Ryan E. Da Re, J. D. Thompson, Jaqueline L. Kiplinger, David E. Morris, and Kevin D. John*

Los Alamos National Laboratory, Los Alamos, New Mexico 87545

Received January 25, 2008

A new complex, $Cp^*_2Sm(tpy)$ (**1**, where $Cp^* = C_5Me_5$, tpy = 2,2′:6′,2″-terpyridine) and its one-electron oxidized congener $[Cp^*_2Sm(tpy)]PF_6$ ($[\mathbf{1}]^+$) have been synthesized and characterized with the aim of comparing their electronic and magnetic behavior to the known ytterbium analogues: $Cp^*_2Yb(tpy)$ (**2**) and $[Cp^*_2Yb(tpy)]OTf$ ($[\mathbf{2}]^+$). These new samarium complexes have been characterized using single-crystal X-ray diffraction, ^1H NMR spectroscopy, cyclic voltammetry, optical spectroscopy, and bulk magnetic susceptibility measurements. All data for **1** indicate a Sm(III)−tpy$^{\bullet\,-}$ $[(4f)^5-(\pi^*)^1]$ ground-state electronic configuration similar to that found previously for **2** $[(4f)^{13}-(\pi^*)^1]$. Structural comparisons reveal that there are no significant changes in the overall geometries associated with the neutral and cationic samarium and ytterbium congeners aside from those anticipated based upon the lanthanide contraction. The redox potentials for the divalent $Cp^*_2Ln(THF)_n$ precursors ($E_{1/2}(Sm^{2+}) = -2.12$ V, $E_{1/2}(Yb^{2+}) = -1.48$ V) are consistent with established trends, the redox potentials (metal-based reduction and ligand-based oxidation) for **1** are nearly identical to those for **2**. The correlation in the optical spectra of **1** and **2** is excellent, as expected for this ligand−radical based electronic structural assignment, but there does appear to be a red-shift (∼400 cm^{-1}) in all of the bands of **1** relative to those of **2** that suggests a slightly greater stabilization of the π^* level(s) in the samarium(III) complex compared to that in the ytterbium(III) complex. Similar spectroscopic overlap is observed for the monocationic complexes $[\mathbf{1}]^+$ and $[\mathbf{2}]^+$. Bulk magnetic susceptibility measurements for **1** reveal significantly different behavior than that of **2** due to differences in the electronic-state structure of the two metal ions. The implications of these differences in magnetic behavior are discussed.

Introduction

Our group[1] and others[2] have studied polypyridyl adducts of ytterbium metallocenes including $Cp^*_2Yb(tpy)$ ($Cp^* = C_5Me_5$, tpy = 2,2′;6′,2″-terpyridine) (**2**) to better understand the nature of the charge-transfer ground state $[(4f)^{13}-(\pi)^{*1}]$ and subsequent impact on the electronic and magnetic behavior associated with these molecular species. Interpretation of magnetic data in these systems is contingent on the existence of two spin contributions, the ytterbium(III) center ($J = {}^7/_2$), and the ligand radical ($S = {}^1/_2$). The description of the electronic wave functions and the nature of the coupling between these two spins remains a topic of intense analysis, having been studied by a variety of techniques including SQUID magnetometry[1,2] and X-ray absorption spectroscopy.[2d] In particular, these monometallic complexes exhibit a temperature-dependent magnetic behavior that departs dramatically from the Curie law. The nature of this behavior appears to derive from a strong ($>10^2$ cm^{-1}) coupling interaction between the two spin centers observed in the neutral complex, given that the one-electron oxidized congeners, for example, $Cp^*_2Yb(tpy)^+$ ($[\mathbf{2}]^+$), exhibit mag-

* To whom correspondence should be addressed. E-mail: kjohn@lanl.gov.

(1) (a) Carlson, C. N.; Veauthier, J. M.; John, K. D.; Morris, D. E. *Chem.—Eur. J.* **2008**, *14*, 422–431. (b) Veauthier, J. M.; Schelter, E. J.; Kuehl, C. J.; Clark, A. E.; Scott, B. L.; Morris, D. E.; Martin, R. L.; Thompson, J. D.; Kiplinger, J. L.; John, K. D. *Inorg. Chem.* **2005**, *44*, 5911–5920. (c) Da Re, R. E.; Kuehl, C. J.; Brown, M. G.; Rocha, R. C.; Bauer, E. D.; John, K. D.; Morris, D. E.; Shreve, A. P.; Sarrao, J. L. *Inorg. Chem.* **2003**, *42*, 5551–5559. (d) Kuehl, C. J.; Da Re, R. E.; Scott, B. L.; Morris, D. E.; John, K. D. *Chem. Commun.* **2003**, 2336–2337.

(2) (a) Walter, M. D.; Berg, D. J.; Andersen, R. A. *Organometallics* **2007**, *26*, 2296–2307. (b) Walter, M. D.; Berg, D. J.; Andersen, R. A. *Organometallics* **2006**, *25*, 3228–3237. (c) Walter, M. D.; Berg, D. J.; Andersen, R. A. *New J. Chem.* **2006**, *30*, 238–246. (d) Booth, C. H.; Walter, M. D.; Daniel, M.; Lukens, W. W.; R; Andersen, R. A. *Phys. Rev. Lett.* **2005**, *95*, 267202. (e) Schultz, M.; Boncella, J. M.; Berg, D. J.; Tilley, T. D.; Andersen, R. A. *Organometallics* **2002**, *21*, 460–472. (f) Berg, D. J.; Boncella, J. M.; Andersen, R. A. *Organometallics* **2002**, *21*, 4622–4631.

10.1021/ic8001465 CCC: $40.75
Published on Web 06/10/2008

netic behavior of the ytterbium(III) ion exclusively. Additionally, the low-temperature magnetic moments of these complexes become vanishingly small, belying a simple ground state resulting from antiferromagnetic coupling of the spins together with ytterbium(III) crystal field effects. This behavior has been equated to a screening of the f moment by the π electrons of the polypyridyl ligand, similar to the Kondo effect observed in solids.[3]

In an attempt to better understand the electronic structure in these polypyridyl adducts of lanthanide metallocene complexes, we have expanded upon our studies of $Cp^*_2Yb(tpy)$ (**2**) complexes to consider the samarium analogue $Cp^*_2Sm(tpy)$ (**1**) and its one-electron oxidized congener $[Cp^*_2Sm(tpy)]PF_6$ ($[\mathbf{1}]^+$). Previous work on the structurally similar complex $Cp^*_2Sm(bpy)$ revealed that it possessed ^{13}C NMR chemical shifts consistent with a samarium(III) center and exhibited optical absorptions consistent with a bipyridyl anion.[4] Although no temperature-dependent magnetic data were reported for $Cp^*_2Sm(bpy)$, the optical and NMR spectroscopy data suggested that the synthesis of the terpyridyl complex would provide a charge-transfer ground state analogous to the ytterbium species. In the case of samarium, the charge-transfer ground state would result in a $[(4f)^5-(\pi^*)^1]$ configuration. Together with ytterbium, cerium, and others, samarium represents one of the lanthanides that afford multiple oxidation states under mild conditions.[5] As with many intermetallic compounds of cerium and ytterbium,[6] samarium solid-state materials are known to possess ground-state wave functions comprised of multiple electronic configurations, for example, SmS.[7] Our expectation was that substitution of ytterbium(III), $J = {}^7/_2$, by a different redox-active lanthanide such as samarium(III), $J = {}^5/_2$, would provide new insight into the nature of the ground-state wave function and the magnetic coupling interactions that exist in the ytterbium species.

Herein, we report the structural characterization of the samarium complexes $Cp^*_2Sm(tpy)$ (**1**) and $[Cp^*_2Sm(tpy)]PF_6$ ($[\mathbf{1}]^+$) and compare and contrast the electrochemical, electronic, and magnetic behavior of these complexes with their ytterbium analogues, **2** and $[\mathbf{2}]^+$.

Experimental Section

General Procedures. All reactions and product manipulations were carried out under an atmosphere of argon using standard dry box or Schlenk techniques at room temperatures unless otherwise stated. Anhydrous toluene, hexanes, tetrahydrofuran (THF), and *n*-pentane were purchased from Aldrich and stored over 4 Å molecular sieves prior to use. Anhydrous methylene chloride was purchased from Acros and stored over 4 Å molecular sieves prior to use. Deuterated solvents were purchased from Cambridge Isotope Laboratories and purified by passage through a short plug of activated alumina and storage over 4 Å molecular sieves prior to use. The following compounds were prepared according to literature procedures: $Cp^*_2Yb(tpy)$ (**2**),[1b] $[Cp^*_2Yb(tpy)]PF_6$ ($[\mathbf{2}]^+$),[1b] $Cp^*_2Sm(THF)_2$,[8] and $(C_5Me_4Et)_2Sm(THF)_2$.[9] $[Cp_2Fe]PF_6$, 2,2′:6′,2″-terpyridine (tpy), $Sm(OTf)_3$, and SmI_2 were purchased from Aldrich and used as received. Paratone-N (Hampton Research) was purchased from Fisher Scientific and was used as received.

Optical spectra were recorded on a Cary 500 Scan UV−vis/NIR or PerkinElmer Lambda 950 spectrometer. Elemental analyses were performed by Midwest Microlabs. Variable-temperature NMR spectra were recorded on a Bruker Avance 400 MHz spectrometer.

Preparation of $Cp^*_2Sm(tpy)$ (1). A 20 mL glass scintillation vial was equipped with a stir bar and charged with $Cp^*_2Sm(THF)_2$ (193 mg, 0.342 mmol) and toluene (10 mL). To this purple solution was added one equiv of 2,2′:6′,2″-terpyridine (79.6 mg, 0.341 mmol). The resulting dark-green colored solution was stirred for 12 h at room temperature, followed by filtration through a medium porosity frit and removal of the solvent to give a dark-green powder. Next, the powder was dissolved in toluene, filtered through Celite, concentrated to 10 mL, and placed in a −30 °C freezer overnight to give dark-green X-ray quality crystals of $Cp^*_2Sm(tpy)$ (**1**) (72.0 mg, 0.110 mmol, 35%). A second crop of crystals can be obtained by concentrating the mother liquor. The combined yield was 75% (167 mg, 0.255 mmol). Anal. Calcd for $C_{35}H_{41}N_3Sm$: C, 64.27; H, 6.32; N, 6.42. Found: C, 64.20; H, 6.23; N, 6.43. ^1H NMR (400.13 MHz, 20 °C, toluene-d_8): δ 13.2 (2H, tpy-H), 2.42 (30H, Cp*), 0.329 (2H, tpy-H), −16.1 (2H, tpy-H), −68.8 (2H, tpy-H), −119 (2H, tpy-H), −326 (1H, tpy-H). $^{13}C\{^1H\}$-NMR (100.61 MHz, 25 °C, toluene-d_8): δ 138 (Cp^*-C_{ring}), 5.10 (Cp^*-CH_3).

Preparation of $[Cp^*_2Sm(tpy)]PF_6$ ($[\mathbf{1}]^+$). A 20 mL scintillation vial equipped with a stir bar was charged with $Cp^*_2Sm(tpy)$ (**1**) (30 mg, 0.046 mmol) and THF (10 mL). To this dark-green solution was added one equiv of $[Cp_2Fe]PF_6$ (15.0 mg, 0.045 mmol), and the reaction mixture was stirred for 12 h at room temperature to give a bright-orange precipitate. The mixture was filtered through a medium porosity glass frit and the orange precipitate washed with toluene (5−10 mL). Next, the orange powder was redissolved in methylene chloride, filtered through Celite, and the volatiles removed under reduced pressure to give $[Cp^*_2Sm(tpy)]PF_6$ ($[\mathbf{1}]^+$) as an analytically pure orange powder (29.2 mg, 0.0365 mmol, 81%). X-ray quality crystals of $[\mathbf{1}]^+$ were grown from slow vapor diffusion of *n*-pentane into a concentrated methylene chloride solution of $[\mathbf{1}]^+$. Anal. Calcd for $C_{35}H_{41}F_6N_3PSm$: C, 52.61; H, 5.17; N, 5.26. Found: C, 51.91; H, 5.12; N, 5.27. ^1H NMR (400.13 MHz, 20 °C, CD_2Cl_2): δ 7.75 (t, 1H, tpy-H4′), 7.60 (t, 2H, tpy-H4 and tpy-H4″), 7.51 (d, 2H, tpy-H3′ and tpy-H5′), 7.49 (d, 2H, tpy-H3 and tpy-H3″), 6.86 (t, 2H, tpy-H5 and tpy-H5″), 4.02 (d, 2H, tpy-H6 and tpy-H6″), 1.01 (s, 30H, Cp*). $^{13}C\{^1H\}$-NMR (100.61 MHz, 25 °C, CD_2Cl_2): δ 154, 153, 152, 143, 142, 124, 122, 121, 115 (Cp^*-C_{ring}), 15.5 (Cp^*-CH_3).

Electrochemistry. Cyclic voltammetric studies were conducted in an inert atmosphere drybox (argon or nitrogen) using a PerkinElmer Princeton Applied Research Corporation (PARC) Model 263 potentiostat under computer control using M270 software. The electrochemical cell was a modified PARC microcell consisting of a ~3 mm platinum disk working electrode, a platinum

(3) Fulde, P. *Electron Correlations in Molecules and Solids*; Springer-Verlag: Berlin, 1991.
(4) Evans, W. J.; Drummond, D. K. *J. Am. Chem. Soc.* **1989**, *111*, 3329–3335.
(5) Cotton, F. A.; Wilkinson, G.; Murillo, C. A.; Bohmann, M. *Advanced Inorganic Chemistry*, 6th ed.; John Wiley & Sons: New York, 1999.
(6) (a) Petrovic, C.; Movshovich, R.; Jaime, M.; Pagliuso, P. G.; Hundley, M. F.; Sarrao, J. L.; Fisk, Z.; Thompson, J. D. *Europhys. Lett.* **2001**, *53*, 354–359. (b) Bauer, E. D.; Booth, C. H.; Lawrence, J. M.; Hundley, M. F.; Sarrao, J. L.; Thompson, J. D.; Riseborough, P. S.; Ebihara, T. *Phys. Rev. B* **2004**, *69*, 125102.
(7) Annese, E.; Barla, A.; Dallera, C.; Lapertot, G.; Sanchez, J. P.; Vankó, G. *Phys. Rev. B* **2006**, *73*, 140409.
(8) Evans, W. J.; Grate, J. W.; Choi, H. W.; Bloom, I.; Hunter, W. E.; Atwood, J. L. *J. Am. Chem. Soc.* **1985**, *107*, 941–946.
(9) Schumann, H.; Glanz, M.; Hemling, H. *New J. Chem.* **1995**, *19*, 491–494.

wire counter electrode, and a silver wire quasi-reference electrode. All experiments were conducted in THF using ~0.1 M [(*n*-Bu)$_4$N][B(C$_6$F$_5$)$_4$] as the supporting electrolyte.[10] Measured potentials were calibrated using the ferrocene/ferrocenium couple. Data were analyzed using the IGOR Pro (Wavemetrics, Inc.) software package on a Macintosh platform.

Magnetic Susceptibility. Magnetic susceptibility data were collected using a Quantum Design Superconducting Quantum Interference Device (SQUID) magnetometer from 2−350 K. The magnetic susceptibility, defined as the sample magnetization M divided by the applied magnetic field H, was measured as a function of temperature at applied fields of 0.1 T. The samples were sealed in a 5 mm Wilmad 505-PS NMR tube along with a small amount of quartz wool, which held the sample near the tube center. Contributions to the magnetization from quartz wool and the NMR tube were measured independently and subtracted from the total measured signal. Diamagnetic corrections for the complexes were made with the use of Pascal's constants.

X-ray Diffraction. Crystals of **1** and [**1**]$^+$ were mounted in a nylon cryoloop using Paratone-N under argon gas flow. The data were collected on a Bruker SMART *APEX II* charge-coupled-device (CCD) diffractometer, with a KRYO-FLEX liquid nitrogen vapor cooling device. The instrument was equipped with a graphite monochromatized Mo Kα X-ray source (λ = 0.71073 Å), with MonoCap X-ray source optics. Data collection and initial indexing and cell refinement were handled using *APEX II* software.[11] Frame integration, including Lorentz-polarization corrections, and final cell parameter calculations were carried out using *SAINT*+ software.[12] The data were corrected for absorption using the *SADABS* program.[13]

The crystal and refinement parameters for **1** and [**1**]$^+$ are listed in Table 1. Selected bond distances and angles are listed in Table 2. Decay of reflection intensity was monitored by analysis of redundant frames. The structures were solved using direct methods and difference Fourier techniques. The hydrogen atoms were refined using a riding model, with their isotropic temperature factors set to 1.2 (aromatic, methyne, methylene) or 1.5 (methyl) times the isotropic U of the attached carbon atom. The final refinement included anisotropic temperature factors on all non-hydrogen atoms. Structure solution, refinement, graphics, and creation of publication materials were performed using *SHELXTL*.[14]

Table 1. Crystal Data and Structure Refinement Parameters for Cp*$_2$Sm(tpy) (**1**) and [Cp*$_2$Sm(tpy)]PF$_6$ ([**1**]$^+$)

	1	[**1**]$^+$
empirical formula	$C_{35}H_{41}N_3Sm$	$C_{35}H_{41}F_6N_3PSm$
fw	654.06	799.03
cryst syst	orthorhombic	monoclinic
space group	*Pbcn*	$P2_1/c$
a, Å	14.540(3)	11.3542(6)
b, Å	14.011(3)	15.1149(8)
c, Å	14.152(3)	19.0997(10)
α, °	90	90
β, °	90	95.867(1)
γ, °	90	90
V, Å^3	2883.1(10)	3260.7(3)
Z	4	4
D_{calcd}, mg/m^3	1.507	1.628
abs. coeff., mm^{-1}	2.065	1.914
F(000)	1336	1612
θ for data collection	2.02 to 29.00	1.72 to 28.97
limiting indices	$-19 \le h \le 19$ $-18 \le k \le 18$ $-18 \le l \le 19$	$-15 \le h \le 15$ $-20 \le k \le 20$ $-24 \le l \le 25$
reflns collected	32 585	38 907
independent reflns	3678 [R(int)=0.0579]	8093 [R(int)=0.0582]
completeness to θ = 25.00°	100.0%	100.0%
refinement method	Full matrix least-squares on F^2	Full matrix least-squares on F^2
data/restraints/params	3678/0/183	8093/0/424
GOF on F^2	1.209	1.063
Final R Indices [$I > 2\sigma I$]	R1 = 0.0259, wR = 0.0606	R1 = 0.0303, wR = 0.0719
R Indices (all data)	R1 = 0.0475, wR2 = 0.0667	R1 = 0.0421, wR2 = 0.0774
largest diff. peak and hole, e·Å^{-3}	1.199 and −0.550	0.858 and −0.605

Table 2. Selected Bond Lengths (Å) and Angles (°) for Cp*$_2$Ln(tpy) and [Cp*$_2$Ln(tpy)]$^+$ (Ln = Sm, Yb)[a]

	Cp*Sm (tpy)**1**	[Cp*$_2$Sm(tpy)] [PF$_6$] [**1**]$^+$	Cp*$_2$Yb (tpy)[b]**2**	[Cp*$_2$Yb(tpy)] [OTf][b] [**2**]$^+$
Ln−Cp*$_{centroid}$	2.504	2.472	2.44	2.38
Ln−N$_{terminal}$	2.498(2)	2.518[2]	2.41(1)	2.433[9]
Ln−N$_{central}$	2.449(3)	2.553(2)	2.42(1)	2.440[9]
Cp*−Ln−Cp*	139.0	142.4	138.3	139.3
N−C−C−N	3	12	1	3

[a] Esd's (standard deviations) are given in parentheses. Values in square brackets are arithmetic means of esd's. [b] Data taken from ref 1b.

Results and Discussion

Synthesis and Structural Characterization. The neutral terpyridine adduct of samarocene was prepared by adding 1 equiv of 2,2′:6′,2″-terpyridine to a solution of Cp*$_2$Sm(THF)$_2$ in toluene and stirring for 12 h at ambient temperature. Dark-green X-ray quality crystals of Cp*$_2$Sm(tpy) (**1**) were grown at −30 °C from toluene (75% yield). **1** undergoes oxidation with ferrocenium hexafluorophosphate in THF to give [Cp*$_2$Sm(tpy)]PF$_6$ ([**1**]$^+$) as a bright-orange analytically pure powder in 81% yield. X-ray quality crystals of [**1**]$^+$ were grown by diffusion of *n*-pentane into a methylene chloride solution of [**1**]$^+$.

The ^{13}C NMR chemical shifts of the Cp* carbon atoms of **1** (δ 138 and 5.10) are consistent with oxidation of samarium(II) to samarium(III) to form a nominal [(4f)^5−(π*)^1] complex. Evans and co-workers examined the ambient-temperature ^{13}C NMR spectra of several decamethyl samarocene complexes and observed chemical shifts between δ 113−121 (***C*****$_5$**Me$_5$) and between δ 18−28 (C$_5$***Me*****$_5$**) at room temperature for the trivalent samarium complexes, whereas chemical shifts for the divalent complexes were observed between −79 to −99 ppm (***C*****$_5$**Me$_5$) and between δ 94 to 100 (C$_5$***Me*****$_5$**).[15] For the related bipyridine complex Cp*$_2$Sm(bpy), the Cp* ligand carbons are reported to resonate at δ 136 (***C*****$_5$**Me$_5$) and δ 9.0 (C$_5$***Me*****$_5$**). We also note that Evans et al. do not report observed chemical shifts for the bipyridyl carbons of Cp*$_2$Sm(bpy).[4] Likewise, we do not observe the terpyidyl carbons in ^{13}C NMR spectra of **1**.

(10) (a) LeSuer, R. J.; Geiger, W. E. *Angew. Chem., Int. Ed.* **2000**, *39*, 248–250. (b) Camire, N.; Mueller-Westerhoff, U. T.; Geiger, W. E. *J. Organomet. Chem.* **2001**, *637−639*, 823–826.
(11) *APEX II 1.08*; Bruker AXS, Inc.: Madison, WI, 2004.
(12) *SAINT+ 7.06*; Bruker AXS, Inc.: Madison, WI, 2003.
(13) *SADABS 2.03*; George Sheldrick: University of Göttingen: Göttingen, Germany, 2001.
(14) *SHELXTL 5.10*; Bruker AXS, Inc.: Madison, WI, 1997.
(15) (a) Evans, W. J.; Ulibarri, T. A. *J. Am. Chem. Soc.* **1987**, *109*, 4292–4297. (b) Evans, W. J.; Hughes, L. A.; Hanusa, T. P. *Organometallics* **1986**, *5*, 1285–1291.

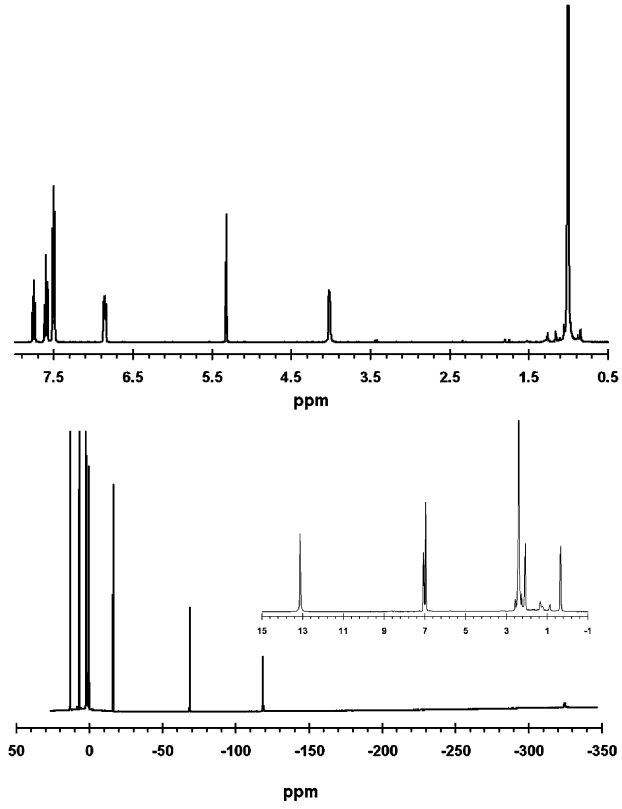

Figure 1. ^{1}H NMR spectra of $Cp^*_2Sm(tpy)$ (**1**) (bottom, toluene-d_8) and $[Cp^*_2Sm(tpy)]PF_6$ ($[\mathbf{1}]^+$) (top, CD_2Cl_2) at 400 MHz and room temperature.

However, oxidation of **1** to $[\mathbf{1}]^+$ (i.e., $[(4f)^5-(\pi^*)^1] \rightarrow [(4f)^5-(\pi^*)^0]$) allows us to observe ^{13}C resonances for the two sets of Cp* carbons (δ 115 and 15.5) and also those of the eight unique terpyridyl carbons (δ 154, 153, 152, 143, 142, 124, 122, and 121) of $[\mathbf{1}]^+$.

The ^{1}H NMR spectra for **1** and $[\mathbf{1}]^+$ are shown in Figure 1. At ambient temperatures, the protons for the $[(4f)^5-(\pi^*)^1]$ configured samarium(III) complex (**1**) resonate in a large chemical shift window (δ 15 to -330). Although the methyl protons of the Cp* ligand (δ 2.3) are not significantly shifted from normal, the terpyidyl protons experience exceedingly large paramagnetic shifts with a single resonance appearing as far upfield as δ -325. In contrast, the protons of the $[(4f)^5-(\pi^*)^0]$ samarium(III) complex ($[\mathbf{1}]^+$) all resonate in a typical NMR chemical shift window (δ 8.0 to 0.0). This would suggest that the large shifts associated with the terpyridyl protons of **1** are dominated by the ligand radical rather than the paramagnetic samarium(III) center. There are some notable differences when these spectra are compared to those of the ytterbium analogues **2** and $[\mathbf{2}]^+$. First, the terpyridyl protons of the $[(4f)^{13}-(\pi^*)^1]$ configured ytterbium(III) complex (**2**) also experience strong paramagnetic shifts at ambient temperatures (δ 100.0 and -50.0).[1b] Unlike the oxidized samarium(III) complex ($[\mathbf{1}]^+$) (chemical shifts between δ 8.0 and 0.0), the chemical shifts of the oxidized ytterbium(III) complexes ($[\mathbf{2}]^+$) experience strong paramagnetic shifts such that they reside between δ 70.0 and -3.0.

The differences in NMR spectra between these samarium and ytterbium systems reflect the different magnetic moments and crystal field effects of the associated Ln(III) metals ($J = {}^7/_2$, μ_{eff} (Calcd) = 4.3 μ_B for ytterbium; $J = {}^5/_2$, μ_{eff} (Calcd) = 1.58 μ_B for samarium), which result in differences in the magnetic moments of **1** and **2**. Because these effects should be temperature dependent, variable-temperature ^{1}H NMR spectra were obtained for **1,** $[\mathbf{1}]^+$, **2**, and $[\mathbf{2}]^+$. Plots of δ versus T^{-1} for **1**, $[\mathbf{1}]^+$, **2**, and $[\mathbf{2}]^+$ are available as Supporting Information. In general, the Cp* protons of these complexes vary little with temperature. However, we observe a strong temperature dependence for the terpyridyl protons in the charge-transfer complexes, **1** ($\Delta\delta$ > 100 ppm for a single resonance) and **2** ($\Delta\delta$ > 50 ppm for a single resonance), which is consistent with a more effective transfer of electron density from the samarium(II) metal center to the terpyridyl ligand in **1** versus the ytterbium(II) metal center in **2**. Although not as pronounced as that in **2**, a small temperature dependence is also observed for the resonances of the terpyridyl protons of the oxidized ytterbium complex ($[\mathbf{2}]^+$) ($\delta\Delta$ < 20 ppm for a single resonance), whereas those of the samarium analogue ($[\mathbf{1}]^+$) remain essentially unchanged with temperature. Andersen and co-workers have also reported variable-temperature proton NMR studies on the related ytterbocene bipyridyl complex, $Cp^*_2Yb(bpy)$, and on other similar ytterbocene N-heterocyclic derivatives, which also show a strong temperature dependence for the chemical shifts of the protons of the N-heterocyclic ligands.[2a,b]

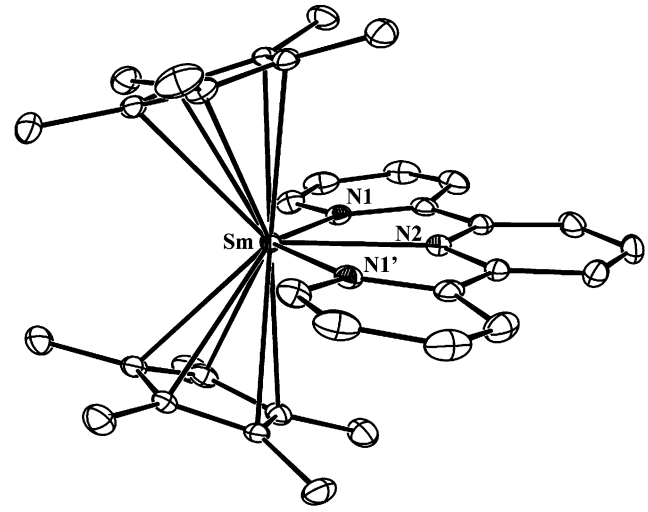

Figure 2. Thermal ellipsoid representation of $Cp^*_2Sm(tpy)$ (**1**) (35% probability ellipsoids). The hydrogen atoms have been removed for clarity.

The X-ray structures of **1** and $[\mathbf{1}]^+$ are shown in Figure 2 and 3, respectively, and selected bond lengths and angles are listed in Table 2. For both **1** and $[\mathbf{1}]^+$, the terpyridine ligands are bound in a tridentate fashion within the samarocene wedge. The overall geometries of **1** and $[\mathbf{1}]^+$ are consistent with these complexes possessing a trivalent samarium metal center. The average $Sm-Cp^*_{cent}$ distances are 2.504 Å for **1** and 2.472 Å for $[\mathbf{1}]^+$. The average $Sm-C_{ring}$ distances are 2.776(3) Å for **1** and 2.746(3) Å for $[\mathbf{1}]^+$ and are within the range of 2.68−2.77 Å for known $Cp^*_2Sm(III)$ complexes and are just outside the range of 2.79−2.86 Å for published $Cp^*_2Sm(II)$ complexes.[16] Evans

(16) Evans, W. J.; Foster, S. E. *J. Organomet. Chem.* **1992**, *433*, 79–94.

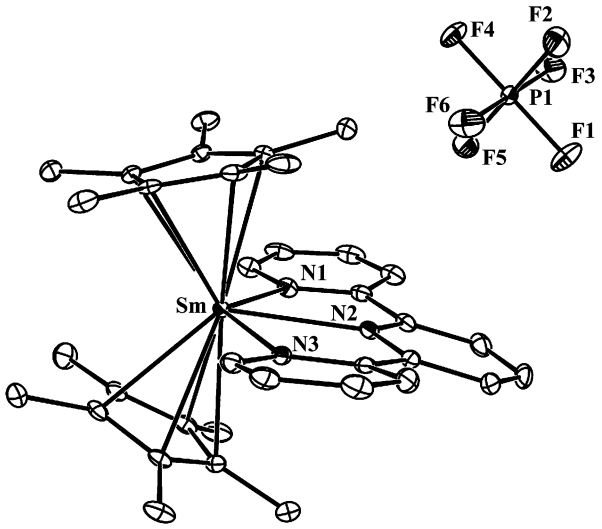

Figure 3. Thermal ellipsoid representation of $[Cp^*_2Sm(tpy)]PF_6$, ($[\mathbf{1}]^+$) (35% probability ellipsoids). The hydrogen atoms have been removed for clarity.

and co-workers report an average Sm−C distance of 2.724(3) Å for the bipyridine complex $Cp^*_2Sm(bpy)$.[4] Additionally, the Cp^*_{cent}−Sm−Cp^*_{cent} angles of 139.0° for **1** and 142.4° for $[\mathbf{1}]^+$ compare well to that of the $Cp^*_2Sm(bpy)$ complex (137.9°). Further comparison of the structures of the neutral and cationic complexes of Cp*Sm(tpy) (**1** and $[\mathbf{1}]^+$) reveals a lengthening of both the central and terminal Sm−N distances upon oxidation of the neutral complex. For example, the Sm−N_{cent} bond distance lengthens from 2.449(3) Å for **1** to 2.553(2) Å for $[\mathbf{1}]^+$. When **1** and $[\mathbf{1}]^+$ are compared to their ytterbium congeners, no gross structural variations are observed from those expected based upon the lanthanide contraction (samarium(III) ionic radius = 0.964 Å; ytterbium(III) ionic radius = 0.858 Å). However, the orientation of the tpy ligand in $[\mathbf{1}]^+$ is such that the central ring is puckered out of the plane defined by the SmN_3 plane by ∼9°, whereas the outer rings are puckered down by ∼6°.

Electrochemistry. Cyclic voltammetric data in ∼0.1 M [(*n*-Bu)$_4$N][$B(C_6F_5)_4$]/THF solution for free tpy, **1**, **2**, $(C_5Me_4Et)_2Sm(THF)_n$ and $Cp^*_2Yb(THF)_n$ are illustrated in Figure 4. Half-wave potential data extracted from these voltammograms are summarized in Table 3. Data could not be obtained for the $Cp^*_2Sm(OEt_2)$ precursor complex under these same experimental conditions because of rapid decomposition, the origin of which is suspected to lie in the reaction of this metallocene with the fluoroarylborate electrolyte anion, $[B(C_6F_5)_4]^-$. However, as illustrated in Figure 4, the structurally related $(C_5Me_4Et)_2Sm(OEt_2)$ complex was found to be sufficiently stable to enable collection of the voltammetric data. In THF solution, the complex does undergo a facile THF for OEt_2 exchange reaction, evidenced by a pronounced color change (green to red) as reported previously for the $Cp^*_2Yb(OEt_2)$ complex.[1c] However, we do not expect these relatively minor structural variations in either the cyclopentadienyl ligand or the solvent adduct to have a substantial impact on the redox potentials, and thus believe the reported samarium(III)/samarium(II) half-wave potential to be a good approximation of that for the Cp^*_2Sm precursor species.

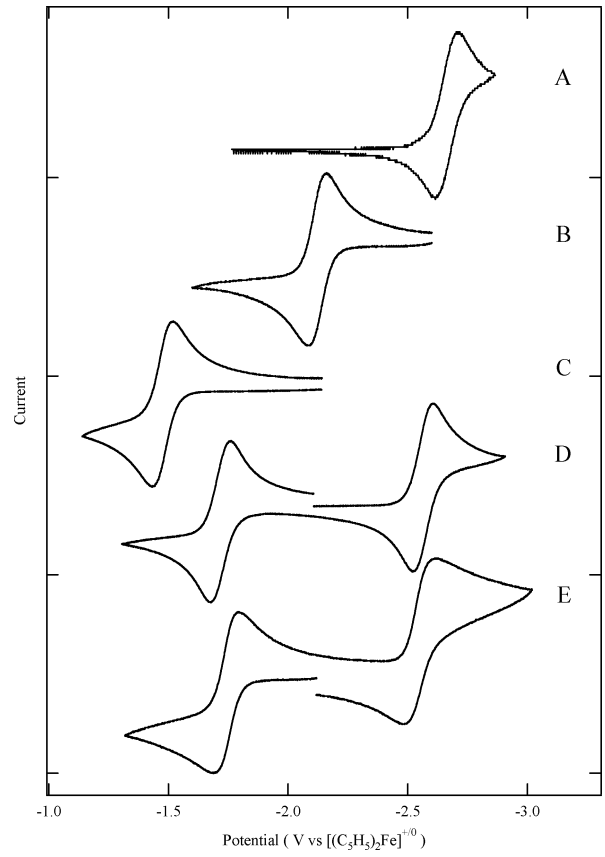

Figure 4. Cyclic voltammograms at a platinum working electrode in ∼0.1 M [(*n*-Bu)$_4$N][$B(C_6F_5)_4$]/THF solution: (A) Free terpyridine, (B) $(C_5Me_4Et)_2Sm(THF)_n$, (C) $Cp^*_2Yb(THF)_n$, (D) $Cp^*_2Yb(tpy)$ (**2**), (E) $Cp^*_2Sm(tpy)$ (**1**). Data for A, C, and D are from ref 1d.

Table 3. Measured Redox Potentials for $Cp^*_2Ln(tpy)$ Adducts and Constituents (Ln = Sm, Yb)[a]

species	$E_{1/2}(L/L^-)$	$E_{1/2}(M^{3+}/M^{2+})$	$\lvert\Delta E_{1/2}\rvert$[b]
tpy	−2.66		
$(C_5Me_5)_2Yb(THF)_n$[c]		−1.48	
$(C_5Me_4Et)_2Sm(THF)_n$		−2.12	
$(C_5Me_5)_2Yb(tpy)$[c] (**2**)	−1.72	−2.56	0.84
$(C_5Me_5)_2Sm(tpy)$ (**1**)	−1.74	−2.55	0.81

[a] All $E_{1/2}$ values are in volts versus $[(C_5H_5)_2Fe]^{+/0}$ in ∼0.1 M [(*n*-Bu)$_4$N][$B(C_6F_5)_4$]/THF. [b] $|\Delta E_{1/2}| = |E_{1/2}(L/L^-) - E_{1/2}(M^{3+}/M^{2+})|$ in volts. [c] Data from ref 1d.

The measured redox potentials (Table 3) for the divalent metal precursors, Cp^*_2Yb and $(C_5Me_4Et)_2Sm$ as THF adducts, follow the same thermodynamic trend known for ytterbium(III)/ytterbium(II) versus samarium(III)/samarium(II) (e.g., in acidic aqueous media), with the latter reduction occurring at ∼0.5 V more negative potential than the former.[17] Of far greater relevance, however, is that formation of the terpyridyl adduct $Cp^*_2Sm(tpy)$ (**1**) induces the same dramatic change in redox energetics as that observed in the Cp^*_2Yb system, and the resultant metal-based reduction and ligand-based oxidation processes are nearly isoenergetic in the two systems. In both systems, the assignment of the voltammetric waves to metal-based reduction and ligand-based oxidation processes is predicated on

(17) Morss, L. R. Yttrium, Lanthanum, and the Lanthanide Elements In *Standard Potentials in Aqueous Solution*; Bard, A. J., Parsons, R., Jordan, J., Eds.; CRC Press: New York, 1985.

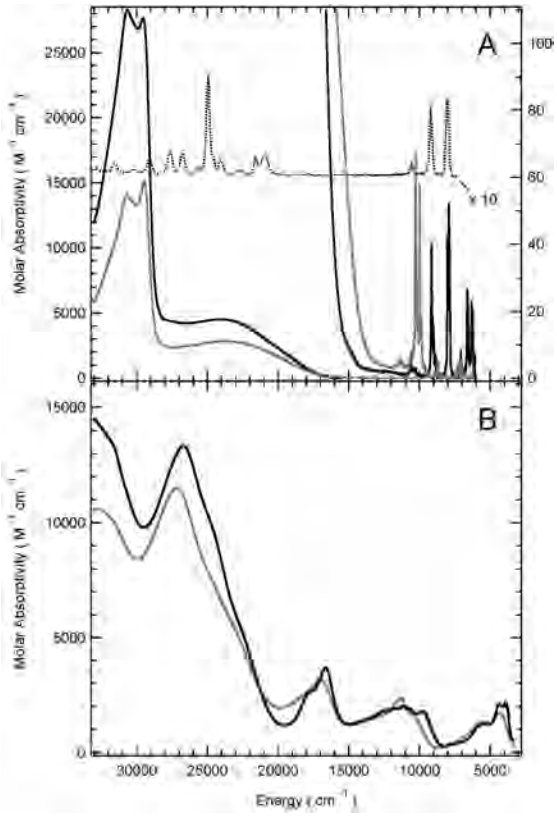

Figure 5. Electronic spectral data for $[Cp^*_2Ln(tpy)]^+$ in CH_2Cl_2 (**A**) and $Cp^*_2Ln(tpy)$ in toluene (**B**). Black lines correspond to Ln = Sm (**1** and $[\mathbf{1}]^+$) and gray lines correspond to Ln = Yb (**2** and $[\mathbf{2}]^+$). The dashed-line spectrum in **A** is for $Sm(OTf)_3$ in H_2O. The right-hand scale in **A** pertains to the narrow band spectra derived from the f−f transitions. Data for **2** and $[\mathbf{2}]^+$ are from refs 1d and 22.

the abundance of other data including optical and NMR spectroscopy and magnetic susceptibility that demonstrate unequivocally that the ground-state electronic configuration in **1** is Sm(III)−tpy$^{\bullet-}$. This renders the tpy radical the most easily oxidized species and the samarium(III) metal center the most easily reduced species.

Electronic Absorption Spectroscopy. UV−vis−near IR absorption spectra were obtained for **1** and $[\mathbf{1}]^+$ in toluene and CH_2Cl_2 solution, respectively. Spectra are illustrated in Figure 5 in comparison to the data obtained previously for **2** and $[\mathbf{2}]^+$. Data are also included in Figure 5 of $Sm(OTf)_3$ in H_2O to illustrate the nominal metal-based intraconfiguration (f−f) transitions typical of this $4f^5$ metal ion.

Cationic Species. The spectra for the cationic complexes $[\mathbf{1}]^+$ and $[\mathbf{2}]^+$ clearly exhibit two distinct spectral regions. The first in the UV−vis range consists of two groups of transitions, one at energies greater than ∼28 000 cm^{-1} and the other in the range from ∼15 000−28 000 cm^{-1}, and each is comprised of fairly broad, intense bands. The second is in the NIR spectral range and is comprised of a series of much narrower, relatively low intensity bands.

The correlation in the band energies and profiles in the spectra for $[\mathbf{1}]^+$ and $[\mathbf{2}]^+$ in the UV−vis region is pronounced and indicates that the assignments for the transitions giving rise to these bands must be similar for both complexes. The highest energy set of bands is assigned to $\pi-\pi^*$ transitions localized on the tpy ligand. Bands having comparable energies and intensities have been reported previously for transition-metal complexes of tridentate polypyridyl ligands.[18] The set of bands in the UV−vis region between ∼15 000−28 000 cm^{-1} for $[\mathbf{1}]^+$ is poorly resolved, but at least two bands can be discerned; the main band with a resolved maximum at ∼24 000 cm^{-1} and an unresolved shoulder that lies to lower energy (∼19 000 cm^{-1}). A similar set of two bands can be seen in the spectrum of $[\mathbf{2}]^+$, and these have been previously assigned as ligand-to-metal charge-transfer (LMCT) in nature.[1c,19] Specifically, the higher-energy, resolved band is assigned to a $\pi_{tpy} \rightarrow 4f_{Ln(III)}$ transition comparable to the LMCT transitions observed for trivalent transition-metal polypyridyl complexes.[20] The unresolved shoulder at lower energy has been assigned to the corresponding $\pi_{Cp^*} \rightarrow 4f_{Ln(III)}$ transition on the basis of assignments of bands having similar energies and intensities in the spectra for a series of Cp^*_3Yb and $Cp^*_3Yb(L)$ [L = THF, PEt_3, etc.] complexes.[21] These assignments made for the spectra of $[\mathbf{2}]^+$ are also plausible for the spectra of $[\mathbf{1}]^+$, although it is interesting that there is such a strong energy correlation in these bands between the $4f^{13}$ ytterbium(III) and $4f^5$ samarium(III) systems.

The narrow bands observed for $[\mathbf{1}]^+$ in the NIR spectral region (part A of Figure 5) are clearly attributable to samarium(III)-based f−f transitions derived from the $4f^5$ valence electronic configuration on the basis of the linewidths and the relatively low oscillator strengths. In particular, note that there is an excellent energy correlation in the spectral region just below 10 000 cm^{-1} for the bands observed in the aquated cation $Sm(H_2O)_n^{3+}$ (prepared from the triflate salt) and those of $[\mathbf{1}]^+$. However, it is noteworthy that the intensities in these f−f bands for $[\mathbf{1}]^+$ are ∼20 times those for the bands in $Sm(H_2O)_n^{3+}$ and are comparable to the intensities found in the f−f bands in this same spectral region for $[\mathbf{2}]^+$. The intensities observed for the f−f bands in $Sm(H_2O)_n^{3+}$ are much more typical of those for intraconfiguration bands in the lanthanide elements and reflect the parity-forbidden nature of these transitions for metal centers in approximately centrosymmetric sites with little interaction between the core-like metal 4f orbitals and the ligands. The enhancement in the f−f intensities observed for the metallocene cations $[\mathbf{1}]^+$ and $[\mathbf{2}]^+$ can be attributed in part to the symmetry reduction to $\sim C_{2v}$ that relaxes the parity selection rule but also to a greater metal f-orbital/ligand-orbital interaction as demonstrated previously for $[\mathbf{2}]^+$ from resonance-enhanced Raman vibrational and vibronically resolved

(18) (a) Stone, M. L.; Crosby, G. A. *Chem. Phys. Lett.* **1981**, *79*, 169–173. (b) Harris, C. M.; McKenzie, E. D. *J. Inorg. Nucl. Chem.* **1963**, *25*, 171–174.

(19) Da Re, R. E.; Kuehl, C. J.; Donohoe, R. D.; John, K. D.; Morris, D. E. *Electronic Spectroscopy of [(C5Me5)2 Yb(L)] + (L = 2,2′-bipyridine and 2,2′:6′,2″-terpyridine). Vibronic Coupling and Ligand-field Splitting in the 4f13-Derived Ground and Excited States of Yb3+*; Los Alamos National Laboratory: Los Alamos, NM, 2005; LA-UR-055249.

(20) (a) Nazeeruddin, M. K.; Zakeeruddin, S. M.; Kalyanasundaram, K. *J. Phys. Chem.* **1993**, *97*, 9607–9612. (b) Bergkamp, M. A.; Gutlich, P.; Netrel, T. L.; Sutlin, N. *J. Phys. Chem.* **1983**, *87*, 3877–3883. (c) Bryant, G. M.; Ferguson, J. E. *Aust. J. Chem.* **1971**, *24*, 275.

(21) Schlesener, C. J.; Ellis, A. B. *Organometallics* **1983**, *2*, 529–534.

electronic absorption and emission data that evidence increased dipole-allowed character in these transitions.[19]

Neutral Species. As observed in $Cp^*_2Yb(tpy)$ (**2**) and all other neutral ytterbocene polypyridyl adducts that we and others have investigated,[1,2] nearly the entire UV−vis−NIR region in the spectrum of $Cp^*_2Sm(tpy)$ (**1**) (part B of Figure 5) is dominated by vibronically resolved $\pi-\pi^*$ and $\pi^*-\pi^*$ transitions localized on the terpyridine radical. These assignments are based on the strong correlation in band energies and intensities between these spectra and those found for the alkali-metal reduced terpyridine radical.[22] The correlation in the spectra of **1** and **2** is excellent as expected for this ligand-radical-based spectral assignment, but there does appear to be a red-shift ($\sim$400 cm^{-1}) in all of the bands of **1** relative to those of **2** that suggests a slightly greater stabilization of the π^* level(s) in the samarium(III) complex compared to that in the ytterbium(III) complex. Although these neutral polypyridyl adducts still possess a formally trivalent lanthanide cation with associated f−f bands similar to those seen in the cationic species ($[\mathbf{1}]^+$), part A of Figure 5), the f−f bands are clearly not a prominent characteristic in the spectra of these neutral complexes. The absence of distinct intraconfiguration bands can be attributed for the most part to the lower transitions intensities in these f−f bands that precludes resolving them from the much more intense ligand-radical-based transitions. It is possible that some of the weak, structured features observed on top of the broadband at $\sim$11 000 cm^{-1} could originate from f−f transitions instead of vibronic structure associated with the $\pi-\pi^*$ and $\pi^*-\pi^*$ transitions, but conclusive assignments are not possible in the absence of other data such as magnetic circular dichroism spectra.

The final additional feature in the spectrum of **1** is the lowest energy set of bands centered at $\sim$5000 cm^{-1}. A nearly identical set of bands is seen for **2** and has been assigned as a vibronically structured LMCT transition, $[(4f)^{13}(\pi^*)^1 \rightarrow (4f)^{14}(\pi^*)^0]$. It is clear on the basis of the essentially identical character of the transition in **1** that a comparable assignment is appropriate, namely, $[(4f)^5(\pi^*)^1 \rightarrow (4f)^6(\pi^*)^0]$. As noted for **2**, this transition is the converse of the process that gives rise to the observed ground-state Sm(III)−tpy$^{\bullet-}$ charge-transfer electronic configuration. The observed energy of this transition is also consistent with the expectation from the redox potential data (Table 3) that show that the energy separation between the ligand-based oxidation and the metal-based reduction (i.e., the two component steps in an LMCT transition) is $\sim$6500 cm^{-1} (0.8 V), with the separation (hence the energy) slightly lower for **1** than for **2**. The spacing between the two most prominent vibronic components in this transition ($\sim$1300 cm^{-1}) is also consistent with the proposed LMCT assignment involving a terpyridine ligand in which the excited-state is less antibonding (i.e., loses π^* electron density) than the ground state. This spectral feature is key because in concert with the electrochemical result, it

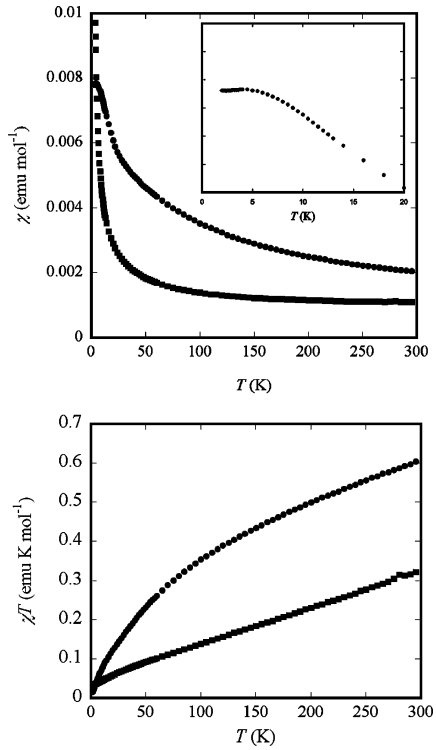

Figure 6. χ vs T (top) and χT vs T (bottom) plots of $Cp^*_2Sm(tpy)$ (**1**, ●) and $[Cp^*_2Sm(tpy)]PF_6$ ($[\mathbf{1}]^+$, ■). The data were measured in an applied field of 0.1 T using solid-state SQUID magnetometry.

establishes the essentially identical orbital energetic landscape between **1** and **2**.

Magnetic Susceptibility. The magnetic susceptibility of **1** and $[\mathbf{1}]^+$ was evaluated to compare to the previously reported ytterbium analogues.[1b] As expected, the susceptibility of $[\mathbf{1}]^+$ shows typical behavior for a simple samarium(III) complex.[23] The high temperature χT product of $[\mathbf{1}]^+$ achieves a value of 0.33 emu K mol^{-1} at 300 K, which is typical for this $J = {}^5/_2$ ($^6H_{5/2}$) ion (Figure 6).[23] The χT product of $[\mathbf{1}]^+$ decreases over the whole temperature range and is fairly linear, indicative of temperature independent paramagnetism in the complex. The neutral **1** exhibits a χT product of 0.61 emu K mol^{-1} at 300 K, similar to the reported value of 0.72 emu K mol^{-1} for $Cp^*_2Sm(bpy)$, which was determined by the Evans method.[4] The value of 0.61 emu K mol^{-1} is consistent with a formulation of a $J = {}^5/_2$ samarium(III) ion and uncoupled $S = {}^1/_2$ organic radical at this temperature. The temperature dependent behavior of **1** decreases in χT versus T over much of the temperature range. This behavior arises from samarium(III) crystal field effects and indicates differences between the low symmetry crystal field (CF) states of **1** and $[\mathbf{1}]^+$, as a result of the anionic versus neutral tpy ligand, on the order of kT. The low-temperature χ versus T plot reaches a maximum at $\sim$5 K (Figure 6, top, inset). This behavior is a clear manifestation of Sm(III)−tpy$^{\bullet-}$ magnetic coupling. At 5 K, only the lowest energy $m_J = \pm{}^1/_2$ microstate of the samarium(III) ion is presumed to be populated. Coupling of this f moment antiferromagnetically with the single unpaired spin on the tpy$^{\bullet-}$ ligand results in

(22) Carlson, C. N.; Kuehl, C. J.; Da Re, R. E.; Veauthier, J. M.; Schelter, E. J.; Milligan, A. E.; Scott, B. L.; Bauer, E. D.; Thompson, J. D.; Morris, D. E.; John, K. D. *J. Am. Chem. Soc.* **2006**, *128*, 7230–7241.

(23) Boudreaux, E. A.; Mulay, L. N. *Theory and Applications of Molecular Paramagnetism*; John Wiley & Sons: New York, 1976.

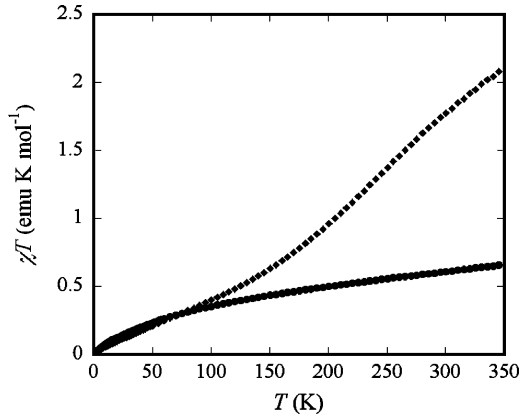

Figure 7. χT vs T plots of $Cp^*_2Sm(tpy)$ (**1**, ●), and $Cp^*_2Yb(tpy)$ (**2**, ■). The data were measured in an applied field of 0.1 T using solid state SQUID magnetometry.

nearly complete cancelation, hence the observation of a maximum in χ versus T. The small radial extent and orbital overlap of the 4f orbitals of the samarium(III) ion result in the weak direct exchange interaction observed for this complex.

The susceptibility data for $Cp^*_2Sm(tpy)$ (**1**) is very different than what has been reported for the ytterbium congener $Cp^*_2Yb(tpy)$ (**2**) (Figure 7). In the case of **2**, the susceptibility decreases dramatically from 250−100 K.[1b] Our initial assessment of this behavior was that it arose because of a temperature-dependent change in the valence state from ytterbium(III) to ytterbium(II). However, variable-temperature electronic absorption experiments have since discounted this possibility.[24] Another explanation that has been advanced for the anomalous behavior of $Cp^*_2Yb(tpy)$ (**2**) and related complexes[25] is that of a confined Kondo effect.[2d] In solid-state materials, the Kondo effect is observed when paramagnetic sites antiferromagnetically couple to conduction electrons, resulting in cancelation of the local magnetic moments.[26] In a spatially confined system, the phenomenon can occur for systems of paramagnetic impurities in nanometer-sized metallic grains wherein conduction states become discrete rather than continuous. In these cases, f-element valences become noninteger. The premise follows that, at the limit of confined systems, f moments of single metal ions couple with coordinated conjugated π systems (e.g., $tpy^{\bullet-}$, $bpy^{\bullet-}$, or COT^{2-}), resulting in total cancelation of their moments. Within this framework of a single metal ion, the diminution of the moment occurs by a mechanism of an admixture of a charge-transfer excited state ($Yb(II)-tpy^0$ in the case of **2**) into the ground state, resulting in strong antiferromagnetic spin polarization of the $Yb(III)-tpy^{\bullet-}$ configuration through Hund's rules. The ytterbium(III) spin is also screened by the delocalized electrons of the conjugated π system, resulting in the vanishingly small moment for temperatures less than ∼75 K. In consideration of **1**, however, such a spin polarization mechanism would predict a strong *ferromagnetic* $Sm-tpy^{\bullet-}$ spin−spin interaction because of the less than half-filled 4f configuration of the samarium(II) charge-transfer excited state, that is, the odd electron in the contribution from the samarium(II) configuration resides in an empty primarily 4f orbital. Comparison of the χT products for **1** and **2** (Figure 7) reveals that the strong coupling interaction active in **2** that perturbs the χT product beyond expectation for simple ytterbium(III) single ion effects is not present in **1**, and the primary coupling interaction in **1** is in fact weak and antiferromagnetic (Figure 6).

The UV−vis near IR absorption results described above afford direct comparisons of the energetics of the critical charge-transfer excited states between **1** and **2**. Comparison of the LMCT bands for the back-transfer of the unpaired electron from $tpy^{\bullet-}$ to Ln(III) between **1** and **2** reveals the energies of the vibronically structured features centered ∼5000 cm^{-1} are substantially equivalent between **1** and **2**. In light of the structural similarity between **1** and **2** and energetic similarity of their LMCT transitions, the differences between **1** and **2** can be reduced to their intrinsic differences in the sign and magnitude of spin−orbit coupling constants and their ground terms/CF splittings. Such comparison is critical because spin−orbit coupling affords the admixture that exhibits the mechanism for strong $Ln(III)-tpy^{\bullet-}$ spin coupling. Reported experimental determinations of spin−orbit coupling constants place $\lambda_{Yb(III)} \approx -2940$ cm^{-1} whereas $\lambda_{Sm(III)} \approx +240$ cm^{-1}.[27] Clearly, **1** does not exhibit the same strong, high-temperature spin polarization mechanism and Kondo effect that has been proposed for **2**, despite having a very similar optical electronic structure. In the context of the confined Kondo model, this can be explained by the much smaller spin−orbit coupling constant of samarium(III) that fails to admix the $Sm(II)-tpy^0$ CT excited state. The presence of the effect in **2** and absence in **1** provides a useful set of complexes for rigorous theoretical assessment of the confined Kondo model.

Summary and Conclusions

A new $Cp^*_2Ln(tpy)$ complex (Ln=Sm) and its corresponding monocation have been synthesized and characterized with the aim of better understanding the electronic and magnetic behavior of this class of materials. We have observed that structural and electronic behavior is quite similar between the samarium and ytterbium analogues. Specifically, the direct structural comparisons reveal no significant changes in the overall geometries between **1** versus **2** and $[\mathbf{1}]^+$ versus $[\mathbf{2}]^+$; however, variable-temperature ^1H NMR studies suggest that samarium(II) more effectively transfers electron density to the terpyridyl ligand in **1** compared to ytterbium(II) in **2**. Furthermore, electronic characterization of the neutral complexes **1** and **2** establishes that the orbital energies in both complexes are nearly identical, with a slightly greater stabilization of the π^* level(s) in the samarium(III) complex (**1**) compared to that

(24) Professor Martin L. Kirk (University of New Mexico), Private Communication.
(25) Edelstein, N. M.; Allen, P. G.; Bucher, J. J.; Shuh, D. K.; Sofield, C. D.; Kaltsoyannis, N.; Maunder, G. H.; Russo, M. R.; Sella, A. *J. Am. Chem. Soc.* **1996**, *118*, 13115–13116.
(26) Aeppli, G.; Fisk, Z. *Comments Cond. Mat. Phys.* **1992**, *16*, 155–165.
(27) Carlin, R. L. *Magnetochemistry*; Springer: Berlin, 1986.

in the ytterbium(III) complex (**2**). Magnetic characterization of $[\mathbf{1}]^+$ reveals that the magnetic behavior is dominated by the samarium(III) center similar to that exhibited by the ytterbium(III) center associated with $[\mathbf{2}]^+$. The susceptibility data for **1** is very different than what has been reported for the ytterbium congener **2**, suggesting that the mechanism for magnetic coupling proposed for **2** is not operative in **1**. This difference between **1** and **2** is likely due to the absence of a multiconfigurational ground-state in **1** due to its intrinsically smaller spin−orbit coupling constant.

Acknowledgement. For financial support of this work, we acknowledge LANL (Agnew National Security Postdoctoral Fellowship to J.M.V.; Frederick Reines and Director's Postdoctoral Fellowships to E.J.S.; Glenn T. Seaborg Postdoctoral Fellowships to C.N.C., R.E.D., and E.J.S.), the LANL Laboratory Directed Research & Development program, and the Division of Chemical Sciences, Office of Basic Energy Sciences, Heavy Element Chemistry program.

Supporting Information Available: Full crystallographic details for **1** and $[\mathbf{1}]^+$ are available as CIF files. Variable-temperature NMR spectroscopy data are available for **1**, $[\mathbf{1}]^+$, **2**, and $[\mathbf{2}]^+$. This material is available free of charge via the Internet at http://pubs.acs.org.

IC8001465